Phase transitions in a quasi-two-dimensional system

Ronen Zangi and Stuart A. Rice
Department of Chemistry and The James Franck Institute, The University of Chicago, Chicago, Illinois 60637
(Received 21 May 1998)

We report the results of molecular dynamics simulations of a quasi-two-dimensional system designed to mimic the quasi-two-dimensional colloid suspensions studied by Marcus and Rice [Phys. Rev. E **55**, 637 (1997)]. The simulations duplicate all of the important qualitative findings of Marcus and Rice, in particular the occurrence of first order liquid-to-hexatic and hexatic-to-solid transitions. At higher densities this system also exhibits an isostructural solid-to-solid transition and a buckling transition, both of which are continuous. We find that the dislocation pair, free dislocation, and free disclination concentrations do not satisfy the predictions of the Kosterlitz-Thouless-Halperin-Nelson-Young theory. Our results cast light on the role of the out of plane motion in determining the global character of the phase diagram of a quasi-two-dimensional system, and they require reconsideration of the suggestion by Bladon and Frenkel [Phys. Rev. Lett. **74**, 2519 (1995)] of the character of the driving force for the first order liquid-to-hexatic and hexatic-to-solid transitions.
[S1063-651X(98)02612-9]

PACS number(s): 64.70.Dv

I. INTRODUCTION

It is now well understood that the character and degree of ordering present in a system is dependent on its spatial dimensionality. Indeed, in one- and two-dimensional systems fluctuations can completely destroy long range order of certain types.

The nature of the decay of translational and orientational order in a condensed phase are conveniently described as follows. In a three-dimensional system the amplitude of the envelope of the density-density correlation function of the ordered solid phase has a nonzero constant value in the limit of infinite separation; this behavior defines the characteristic feature of long range positional order. In a two-dimensional system the envelope of the density-density correlation function of the solid phase decays to zero algebraically (i.e., as $r^{-\nu}$) in the limit of infinite separation, which behavior defines the characteristic feature of quasi-long-range order. Arguments for the lack of long range translational order in a two-dimensional solid were first presented in Refs. [1], [2–4], and [5, 6], where it was shown that long wavelength phonon excitations were sufficient to destroy the translational symmetry of the solid in the limit $r\rightarrow\infty$; a rigorous proof of this behavior was later presented by Mermin for the case of inverse power potentials $u(r)=\varepsilon(\sigma/r)^m$, with $m>2$ [7]. Mermin also pointed out that the absence of long range translational order in a two-dimensional solid does not preclude the existence of long range orientational order, characterized by a persistent correlation in the orientations of the local crystallographic axes in the limit $r\rightarrow\infty$. We will refer to the long range order in the orientations of the vectors that connect the centers of nearest neighbor particles as bond orientation order.

One of the consequences of the loss of long range translational order in a two-dimensional solid, first pointed out about 20 years ago, is that the character of the melting transition can be fundamentally different from that of the melting transition in three dimensions. According to the Kosterlitz-Thouless-Halperin-Nelson-Young (KTHNY) theory [8–12], which is based on a description of the two-dimensional solid as a deformable elastic medium with inclusion of the two classes of point topological defects with smallest excitation energy to mediate structural changes, two-dimensional solids melt via sequential continuous phase transitions. The first transition is from the solid with quasi-long-range positional order and long range bond orientation order to a phase with short range positional order and quasi-long-range bond orientation order, the so called hexatic phase. This transition is driven by the dissociation of bound dislocation pairs in the solid. The second transition transforms the hexatic phase to the liquid phase, in which both positional and bond orientation orders have short range; it is driven by the dissociation of individual dislocations to form disclinations. Although it is currently preferred, the transition sequence described is not the only possible mechanism for two-dimensional melting. For example, it is in principle possible for the dislocation unbinding transition to be preempted by grain boundary induced melting, as suggested by Chui [13]. We note that the KTHNY theory of melting in two dimensions is not based on any particular choice of intermolecular potential energy function; it remains valid for any system which can be characterized as a deformable elastic medium.

However, the results of recent simulations of the phase diagram of a two-dimensional assembly of particles, which interact via a pairwise additive potential consisting of a hard core repulsion and a very narrow square well attraction (or a very narrow step repulsion) [14], imply that the mechanism of melting in two dimensions can depend on the nature of the intermolecular potential energy function. Bladon and Frenkel found, for the potential energy function described above, that when the width of the attractive well is less than 6% of the hard disc diameter the system supports two ordered solid phases with the same packing symmetry. The coexistence region of the first order transition between these solid phases ends at a critical point, near which density fluctuations render the solid phases unstable with respect to dislocation unbinding, and the system supports a hexatic phase. For the case when the square well width is close to the limiting value

for which the low density solid phase becomes unstable, the hexatic region can extend to the melting line. When this occurs, the liquid-to-hexatic transition is predicted to be first order while the hexatic-to-solid transition may be either first or second order. An analytic basis for these results was provided by Chou and Nelson [15], who incorporated into the KTHNY theory an explicit solid-to-solid transition. This analysis, which assumes that the elastic energy of the system includes a term descriptive of the strain arising from the change in density associated with an isostructural solid-to-solid transition, is able to account for the essential features of the phase diagram found by Bladon and Frenkel. However, the Chou-Nelson analysis does not provide a microscopic explanation for the observed phase diagram because it assumes, *a priori*, the existence of the isostructural solid-to-solid transition, and incorporates its effects into the system free energy density.

Experimental testing of the KTHNY predictions concerning the character of two-dimensional melting has been limited by the difficulty of preparing systems which are acceptable representatives of the theoretical model [16]. Typical representatives of two-dimensional systems are monolayers supported on a substrate. Nelson and Halperin [9] and Young [11] showed that a weak incommensurate substrate potential only slightly modifies the character of the predicted solid-to-hexatic transition. Among the interesting changes known to be induced by the potential of an ordered substrate are long range bond orientation order in the hexatic phase, and a washing out of the dislocation→disclination unbinding transition when the substrate has sixfold symmetry. Also, if the two-dimensional solid monolayer has a preferred orientation with respect to the supporting substrate, and that orientation is not along a substrate symmetry axis, the melting transition is expected to be Ising-like, corresponding to the two equivalent ways of orienting the two-dimensional solid with respect to a substrate symmetry axis. Notwithstanding these extensions of the theory to include substrate effects, the necessary and sufficient conditions for a real quasi-two-dimensional system to behave as if it were truly two dimensional remain to be established. It is certainly necessary, but not sufficient, that the range of in-plane correlations greatly exceed the range of out-of-plane correlations, and that the interactions between the system and its supporting substrate furnish only a weak perturbation to the properties of the system. In particular, we believe that the extent to which a realization of a two-dimensional system deviates from true two-dimensional character by exploiting some out-of-plane motion can play a crucial role in the mechanism of the melting transition.

With that caveat in mind, we note that experimental studies of the melting of ordered electrons supported on the surface of liquid He [17–19], and of the melting of an ordered array of charged polystyrene spheres between two plates [20–23], are consistent with many of the predictions of the KTHNY theory, but some deviations are observed in individual studies [24]. A few other experimental studies give results sometimes in accord and sometimes not in accord with the KTHNY theory. Recent experimental studies of a quasi-two-dimensional dense assembly of uncharged sterically stabilized polymethylmetacrylate spheres between two plates [25], with an interparticle interaction of the form shown in Fig. 1 (which we call the Marcus-Rice potential),

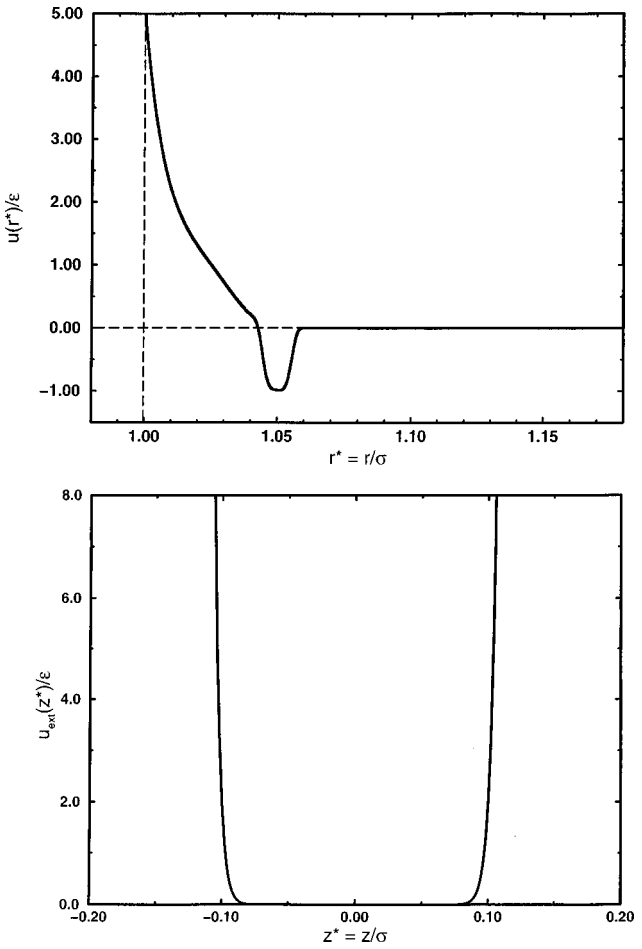

FIG. 1. Marcus-Rice potential as a function of the reduced interparticle distance (top figure), and the external potential as a function of the reduced center of mass coordinate along the vertical axis (z axis) measured from the center of the cell (bottom figure). In both cases, the energy is in units of ε.

have confirmed the inferences of Bladon and Frenkel, i.e., that melting in that system involves sequential first order solid-to-hexatic and hexatic-to-liquid transitions.

Theoretical tests of the KTHNY theory predictions also are abundant [26,27]. An early computer simulation study of two-dimensional melting in a system with Coulomb interactions is consistent with the predictions of the KTHNY theory [28,29], as is a more recent study of a two-dimensional colloid system with Yukawa interactions [30]. The most recent and most extensive computer simulation of the melting of a two-dimensional system of particles which have an interparticle repulsive potential of the r^{-12} form concludes that there are continuous transitions between the solid and hexatic phases and hexatic and liquid phases, but that the density range in which the hexatic phase is stable is very small [31]. Earlier, less definitive, computer simulations of the two-dimensional hard disc system (and of similar systems with short range repulsive interactions) lead to the conclusion that two dimensional melting is a first order transition.

This paper reports the results of extensive computer simulations of a model designed to mimic the system studied by Marcus and Rice [25]. In this model the interaction between spherical particles is represented by a potential like that inferred by Marcus and Rice (see Fig. 1); it has a steeply repulsive core at $r=\sigma$, a soft repulsion in the region $\sigma \leqslant r$

$\leqslant 1.04\sigma$, and a weak attraction in the region $1.04\sigma \leqslant r \leqslant 1.06\sigma$. The spheres are constrained to form a quasi-two-dimensional assembly by a continuous potential acting in the z direction, representing the influence of the cell walls. This potential confines the center of a sphere to be, effectively, within $\pm 0.1\sigma$ of the center plane of the cell. The results of these simulations duplicate all of the important qualitative findings of Marcus and Rice, in particular the occurrence of first order liquid-to-hexatic and hexatic-to-solid phase transitions. We also find that at higher density there is an isostructural solid-to-solid transition, followed by a buckling transition. However, unlike the results of the two-dimensional simulations of Bladon and Frenkel, or the analysis of Chou and Nelson, this isostructural transition is continuous, as is also the buckling transition. We also find that the dislocation pair, free dislocation and free disclination concentrations do not satisfy the KTHNY predictions. Our results cast light on the role of out of plane motion in determining the global character of the phase diagram of a quasi-two-dimensional system, and they require reconsideration of the suggestion by Bladon and Frenkel of the character of the driving force for the first order liquid-to-hexatic and hexatic-to-solid transitions.

II. MODEL SYSTEM AND COMPUTATIONAL DETAILS

The model system studied had 2016 particles contained in a rectangular box with side lengths in the ratio $x:y = 7:(8\sqrt{3}/2)$. We find it convenient to use the reduced variables $r^* = r/\sigma$, $z^* = z/\sigma$, $T^* = k_B T/\varepsilon$, $\rho^* = \rho\sigma^2$, and $m = 1$, with σ the diameter of the particle, ε the depth of the attractive potential well, ρ the number density, and m the mass of the particle. Although the particles can move in the z direction under the influence of a z dependent one body potential (see below), we choose to characterize the state of the system with the two dimensional number density $\rho = N/A$, where A is the area of the simulation cell in the xy plane, since the height of the cell, H, is constant in all of the simulations presented in this paper. Periodic boundary conditions were imposed on the simulation cell in the x and y directions, but not in the z direction. The same number of particles was present in the simulation cell for all of the densities studied. To study the properties of the system with different particle densities, we changed the area of the simulation cell in the xy plane.

The interparticle potential for the model system,

$$u(r^*) = -\varepsilon \exp\left[-\left(\frac{r^* - wc^*}{ww^*}\right)^4\right] + 2\times 10^{-19}\varepsilon\left(r^* - \frac{1}{2}\right)^{-64} + 1.2\varepsilon \exp\left[-\left(\frac{r^* - 0.96}{0.074}\right)^8\right], \tag{2.1}$$

was designed to have the features inferred by Marcus and Rice (see Fig. 1). The first term in Eq. (2.1) represents the attraction between colloid particles when there is incipient overlap between the stabilizing brushes on their surfaces; for simplicity we have taken the functional form of this attraction to be an inverse even power exponent with depth $\varepsilon = 1.0 k_B T$ and width $ww/\sigma = ww^* = 0.006$, centered at $wc^* = 1.05$. The second term in Eq. (2.1) is the core-core repulsion, which is the dominant contribution to $u(r^*)$ when $r^* \leqslant 1$; the functional form chosen is very nearly a hard core repulsion but has continuous derivatives. The last term in Eq. (2.1) is an interpolating soft repulsion, representing the entropy cost associated with interpenetration of the stabilizing brushes attached to the surfaces of the colloid particles; it plays the role of a spline function between the aforementioned attractive and repulsive terms (see Fig. 1). The particles in the model system were also subjected to a one body external potential in the z direction. Consequently, all of the thermodynamic properties of the model system are functions of the strength of this external potential. However, the shape of the potential,

$$u_{ext}(z^*) = \mathcal{D}\varepsilon(z^*)^{\zeta}, \tag{2.2}$$

is such as to confine the system to form a slab with well specified height H, so we can represent its thermodynamic properties with the variables N, T, A, and H in place of N, T, V, and the strength of the external potential. In Eq. (2.2), z^* is the distance from the center of the cell to the center of mass of the particle and $\zeta = 24$ and $\mathcal{D} = 2\times 10^{24}$; this potential confines the particles as if they were in a cell with an effective height of 1.2σ. As is convenient for the purpose at hand, we will sometimes describe the simulation results using reduced units and sometimes using absolute units.

The molecular dynamics (MD) simulations were carried out using the ''velocity Verlet'' algorithm [32], and the Verlet neighbor list method for the calculation of the potential energy [33,34]. The distance at which the potential was cut off was 1.5σ, and the neighbor list cut off was 2.4 times the in plane projected average spacing of the particles. The need for updating of the neighbor list was checked at every time step. The average time step used was, in reduced units, 5×10^{-4}; the associated rms fluctuation in total energy did not exceed one part in 10^5.

The initial configuration for the simulations was taken to be a perfect triangular lattice with all particles located in the plane $z = 0$. The fluid and hexatic phases of the system were equilibrated for 6×10^6 MD steps, and then data collected for 5×10^5 MD steps, every 100 time steps. The solid phases of the system were equilibrated for a longer time; for all densities greater than $\rho^* = 1.130$ the system was equilibrated for at least 10×10^6 MD steps. We checked the achievement of equilibrium by the lack of variation in time of the pressure, energy, and temperature, and of the pair and bond orientation correlation functions.

Since the linear momentum in the z direction is not conserved in our model system (because there is no periodic boundary condition in this degree of freedom), the temperature is related to the kinetic energy K and the total number of degrees of freedom, $3N-2$, by

$$T=\frac{2K}{3N-2}. \tag{2.3}$$

The required temperature was created by multiplication of the velocities by an appropriate constant.

The lateral and transverse pressures, p_l and p_t, respectively, were calculated from the lateral and transverse internal virials $\mathcal{W}_l$ and $\mathcal{W}_t$, where

$$\mathcal{W}_l=-\frac{1}{2}\sum_{i=1}^{N}\sum_{j>i}^{N}\frac{x_{ij}^2+y_{ij}^2}{r_{ij}}\frac{\partial u(r)}{\partial r}\bigg|_{r=r_{ij}}, \tag{2.4a}$$

$$\mathcal{W}_t=-\frac{1}{2}\sum_{i=1}^{N}\sum_{j>i}^{N}\frac{z_{ij}^2}{r_{ij}}\frac{\partial u(r)}{\partial r}\bigg|_{r=r_{ij}}. \tag{2.4b}$$

We find

$$p_l=\frac{Nk_BT+\langle\mathcal{W}_l\rangle}{V}, \tag{2.5a}$$

$$p_t=\frac{Nk_BT+2\langle\mathcal{W}_t\rangle}{V'}, \tag{2.5b}$$

where $V'=Ah$ and $H=\sigma+h$.

Following Landau, a transition between phases is conveniently characterized by an order parameter that is zero in one of the phases (usually taken to be the high temperature phase) and nonzero in the other phase [6]. The order parameter can be defined with respect to the entire system (global order parameter), or it can be defined to take into account only the local environment of a particle (e.g., the nearest neighbor distribution). An abrupt change in the rate of change with density of the global order parameter is a signature of the occurrence of a first order phase transition; in the coexistence region the order parameter is a linear function of the density, a dependence which is equivalent to the lever rule. The behavior of the distribution of local order parameters provides information concerning the nature of the change in structure associated with the phase transition.

The local order parameter descriptive of orientational symmetry in a phase is defined by the projection of the bond orientation onto a local average over the orientations of the bonds to the nearest neighbors:

$$\varphi_{6i}=\frac{1}{n_i}\sum_{j=1}^{n_i}\Psi_{6i}^{*}\Psi_{6j}, \tag{2.6}$$

$$\Psi_{6i}=\frac{1}{n_i}\sum_{j=1}^{n_i}e^{i6\theta_{ij}}. \tag{2.7}$$

In Eqs. (2.6) and (2.7), the sums are taken over the n_i nearest neighbors to particle i, as determined by a two-dimensional Voronoi polygon construction [35,34]. We denote by $\vec{r}_{ij}$ the vector separation of particles i and j, and by θ_{ij} the angle between $\vec{r}_{ij}$ and an arbitrary fixed axis. The global translational order parameter is defined to be the sum of the Fourier components of the density,

$$\Phi_T=\frac{1}{N}\sum_{i=1}^{N}e^{i\vec{G}\cdot\vec{r}_i}, \tag{2.8a}$$

where $\vec{G}$ is a reciprocal lattice vector of the triangular two-dimensional lattice. The corresponding global orientational order parameter is defined by

$$\Phi_6=\frac{1}{N}\sum_{i=1}^{N}\Psi_{6i}. \tag{2.8b}$$

The correlation lengths associated with these order parameters are derived from the decays of the envelopes of the pair distribution function

$$g(r)=\frac{V}{N^2}\left\langle\sum_{i=1}^{N}\sum_{j\neq i}^{N}\delta(\vec{r}-\vec{r}_{ij})\right\rangle, \tag{2.9a}$$

and the bond orientation function

$$G_6(r)=\langle\Psi_6^{*}(0)\Psi_6(r)\rangle, \tag{2.9b}$$

where all the vector and scalar distances are defined to be projections onto the xy plane.

The susceptibilities associated with the translational and orientational order parameters are

$$\chi_T=\frac{N}{T}[\langle\Phi_T^2\rangle-\langle\Phi_T\rangle^2], \tag{2.10a}$$

and

$$\chi_6=\frac{N}{T}[\langle\Phi_6^2\rangle-\langle\Phi_6\rangle^2]. \tag{2.10b}$$

The divergence of these susceptibilities is a signature of the instability of the system, usually interpreted as a change of phase. We note that it has been argued that in a two-dimensional system χ_T can diverge without an instability occurring [36,37].

As is shown in the Appendix, the inherent inhomogeneity of our model system results in different sets of thermodynamic susceptibilities for the lateral and transverse subspaces. The heat capacity per particle at constant A and H is equivalent to the heat capacity at constant volume for a homogenuous system. For the microcanonical ensemble, Lebowitz, Percus, and Verlet showed [38] that the fluctuations in the kinetic energy (or in the potential energy) are related to $c_{A,H}$ by

$$c_{A,H}=\frac{9Nk_B^3T^2}{6Nk_B^2T^2-4\langle\delta K^2\rangle}. \tag{2.11}$$

The lateral and transverse thermal pressure coefficients were calculated from the cross correlation between the fluctuations in the potential energy and the corresponding virials:

$$\gamma_l=\frac{1}{V}\left(Nk_B+\frac{2c_{A,H}\langle\delta\mathcal{U}\delta\mathcal{W}_l\rangle}{3k_B^2T^2}\right), \tag{2.12a}$$

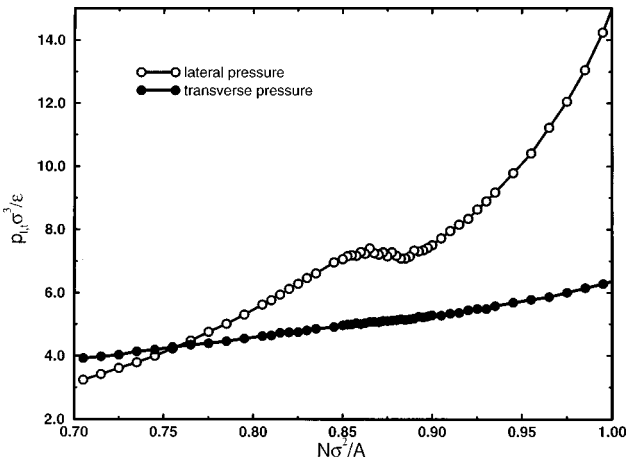

FIG. 2. Lateral pressure (empty circles) and transverse pressure (filled circles) isotherms ($T^*=1$) as a function of the 2D density for the full Marcus-Rice potential.

$$\gamma_t=\frac{1}{V'}\left(Nk_B+\frac{4c_{A,H}\langle\delta\mathcal{U}\delta\mathcal{W}_t\rangle}{3k_B^2T^2}\right). \tag{2.12b}$$

Chou and Nelson showed, from an analytic extension of the KTHNY model, that a two-dimensional isostructural solid-solid transition can involve a rotation of the orientation of one solid phase with respect to the other. We checked for the existence of such a rotation by examining the orientations of the phases with respect to a fixed axis of the Voroni polygons (mostly hexagons) in the solid. The distribution of orientations of the Voroni polygons was represented in terms of the angle ϑ_i defined by

$$\tan(\vartheta_i)=\left(\frac{1}{n_i}\right)\frac{\sum_j^{n_i}\sin(6\theta_{ij})}{\sum_j^{n_i}\cos(6\theta_{ij})}. \tag{2.13}$$

III. RESULTS OF THE SIMULATIONS

All of the simulations reported in this paper refer to a quasi-two-dimensional system with reduced temperature $T^*=1$, and a sample thickness determined by the potential displayed in Eq. (2.2). We will report the results of calculations of the properties of the model system as a function of temperature and sample thickness in another paper.

A. Liquid-to-hexatic and hexatic-to-solid transitions

We consider first the results of simulations using the potential displayed in Fig. 1. Figure 2 displays, for the isotherm $T^*=1$, the lateral pressure and the transverse pressure as a function of density for the range $0.700\leqslant\rho^*\leqslant1.000$. The weak van der Waals loop evident in the lateral pressure isotherm is strong evidence of a coexistence region of a first order transition. This inference is supported by the observation that neither the constant volume heat capacity $c_{A,H}$ (Fig. 3), nor the lateral or transverse thermal pressure coefficient (Fig. 4), is singular in the density region where the van der Waals loop occurs. On the other hand, there is no van der Waals loop in the transverse pressure isotherm, indicating

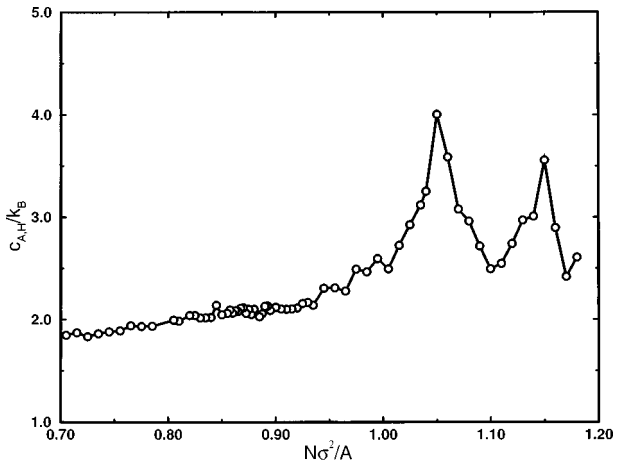

FIG. 3. Heat capacity at constant A and H as a function of the 2D density.

that the transition takes place just in the xy plane. In fact, we find that in the density range $0.850\leqslant\rho^*\leqslant0.900$ there are two first order transitions, namely, liquid to hexatic and hexatic to solid. The identities of the coexisting phases were ascertained from their respective pair correlation and bond orientation correlation functions $g(r^*)$ and $G_6(r^*)$. These functions are displayed in Figs. 5 and 6, respectively, for three sample densities that span the coexistence region, namely $\rho^*=0.900$, 0.870, and 0.850. At the high end of the density range both $g(r^*)$ and $G_6(r^*)$ display behavior characteristic of an ordered solid phase, and at the low end of the density range they both display behavior characteristic of a liquid phase. In the former case the envelope of $g(r^*)$ decays algebraically as $r^*\to\infty$ and the envelope of $G_6(r^*)$ does not decay as $r^*\to\infty$, while in the latter case the envelope of $g(r^*)$ and $G_6(r^*)$ decays exponentially as $r^*\to\infty$. When $\rho^*=0.870$, in the middle of the coexistence region, the envelope of $g(r^*)$ decays exponentially as $r^*\to\infty$, with a falloff that is slower than when $\rho^*=0.850$, and the envelope of $G_6(r^*)$ decays algebraically, with a power law exponent of -0.30, to a nonzero value as $r^*\to\infty$. As shown in Fig. 7, the global translational order parameter Φ_T decays to zero near $\rho^*=0.880$, while the global orientational order

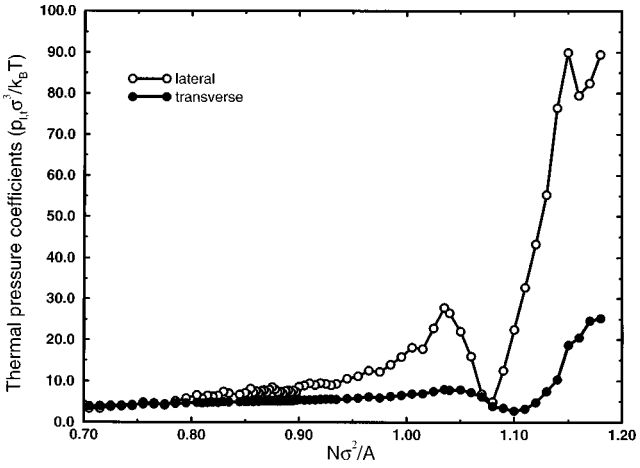

FIG. 4. Lateral (empty circles) and transverse (filled circles) thermal pressure coefficients as a function of the 2D density.

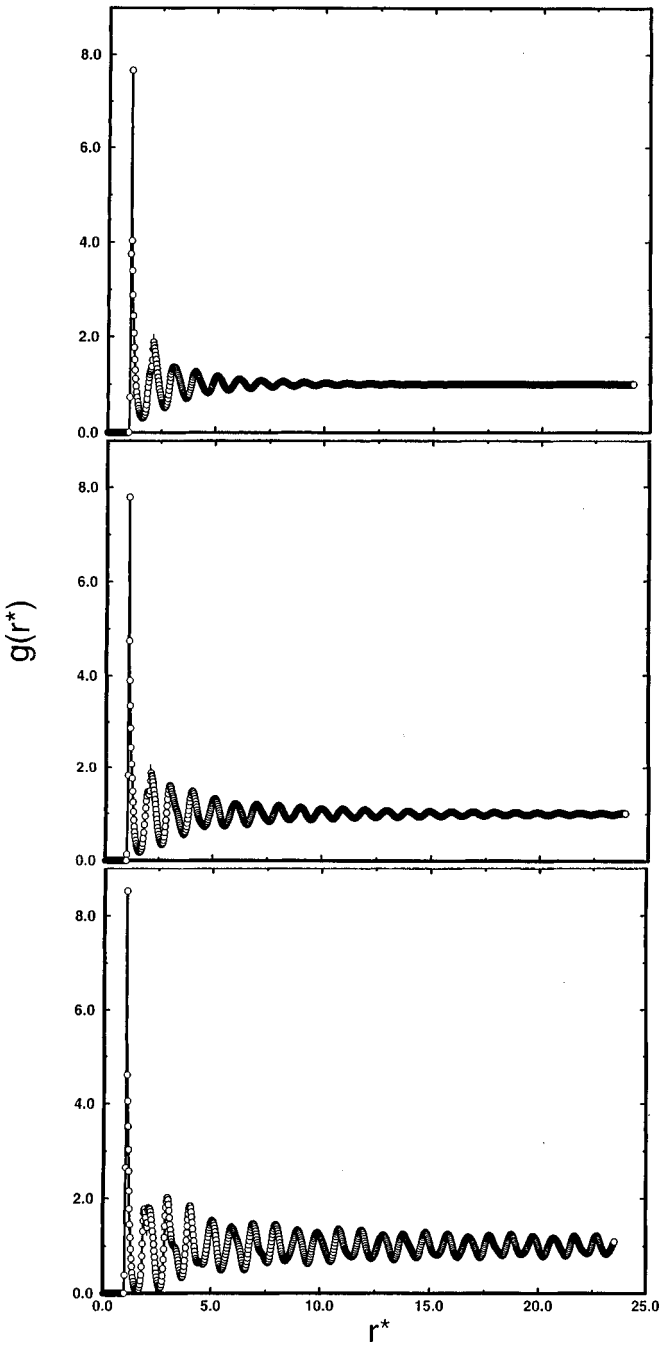

FIG. 5. The pair correlation function of the model system with 2D densities (from top to bottom) 0.850, 0.870, and 0.900.

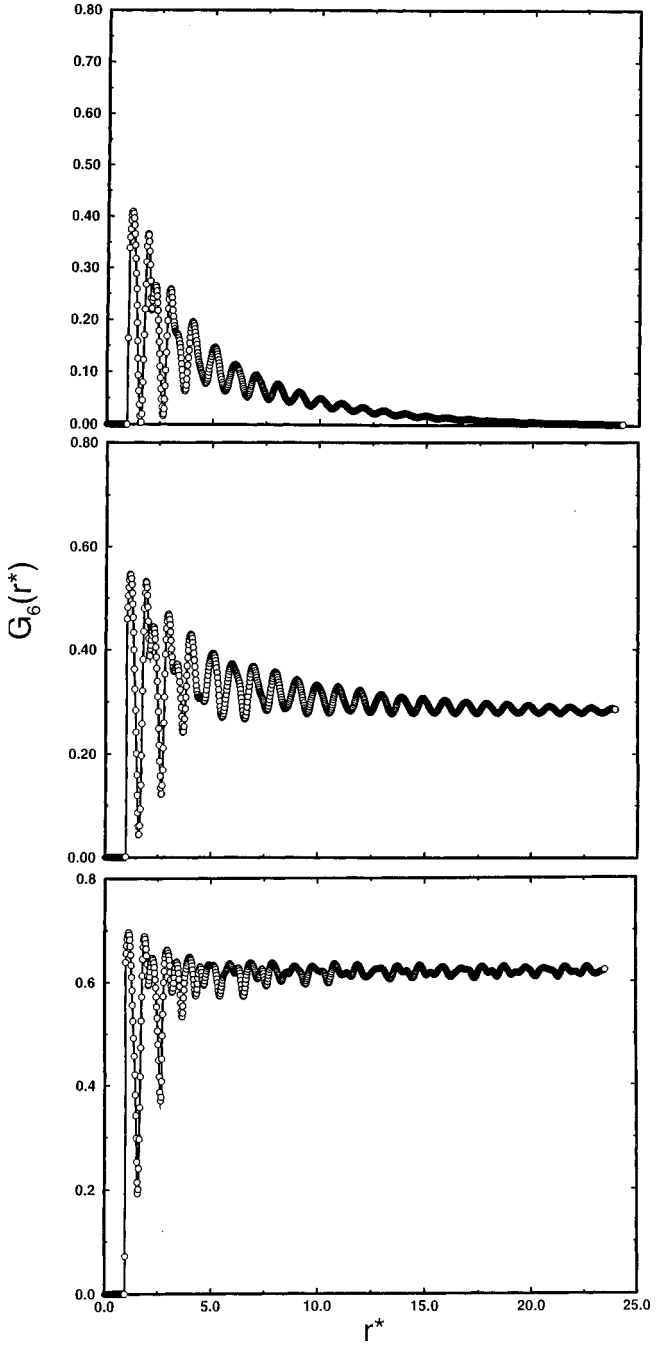

FIG. 6. The bond orientation correlation function of the model system with 2D densities (from top to bottom) 0.850, 0.870, and 0.900.

parameter Φ_6 decays to zero near $\rho^* = 0.850$. Given that the corresponding susceptibilities exhibit singular behavior at those densities (Fig. 8), we infer that between the solid and liquid phases there is another phase, one which has orientational order but no translational order.

The density dependence of the distribution of local orientational order parameters for the liquid phase in the range $0.705 \leqslant \rho^* \leqslant 0.805$ is shown in Fig. 9(a), while the density dependence of the distribution of local orientational order parameters for the solid phase in the range $0.945 \leqslant \rho^* \leqslant 0.995$ is shown in Fig. 9(b). In both the liquid and solid phases the distribution of the local orientational order parameter is unimodal. In the liquid phase that distribution is asymmetric, with a peak at zero for all densities; the asymmetry of the distribution decreases as the density decreases. Since the local orientational order parameter is defined with respect to the angular distribution of bonds to the nearest neighbors of a particle, we expect it to be zero in the liquid phase and nonzero in the hexatic phase. In the solid phase the local orientational order parameter distribution peaks at a value close to 1 at very high density and, as expected for a homogeneous solid, the peak of the distribution shifts continuously to smaller values as the density decreases. The distribution of the local orientational order parameter in the solid phase is markedly less asymmetric than in the liquid phase.

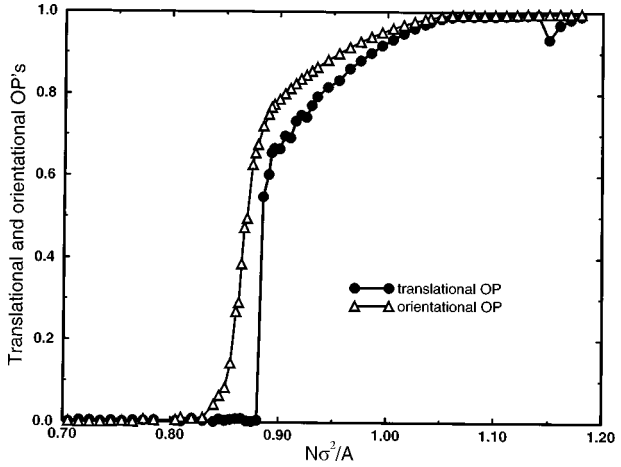

FIG. 7. The global translational (filled circles) and orientation (empty triangles) order parameters as a function of the 2D density.

The density dependence of the distribution of local orientational order parameters for the coexistence region $0.850 \leqslant \rho^* \leqslant 0.900$ is shown in Fig. 10. When $0.890 \leqslant \rho^* \leqslant 0.900$, this distribution is unimodal with a peak at some nonzero value of the order parameter. In contrast, when $0.850 \leqslant \rho^* \leqslant 0.880$ this distribution is bimodal with one peak located at $\varphi_6 = 0$.

The KTHNY theory interprets the mechanism of the predicted two stage continuous melting to involve dissociation of dislocation pairs to form free dislocations followed by the dissociation of free dislocations to form disclinations. In Fig. 11(a) we show the fractions of particles which are five-, six- and seven-coordinated as a function of density, and in Fig. 11(b) the fractions of dislocation pairs, free dislocations, and free disclinations as a function of density. Dislocation pairs first appear in our simulation sample at a density just above the high density end of the van der Waals loop, and free dislocations and free disclinations start to appear just inside the high density end of the van der Waals loop. We do not find any region in which there are free dislocations but no free disclinations, in contrast with the behavior predicted by the KTHNY description of the hexatic phase. The densities

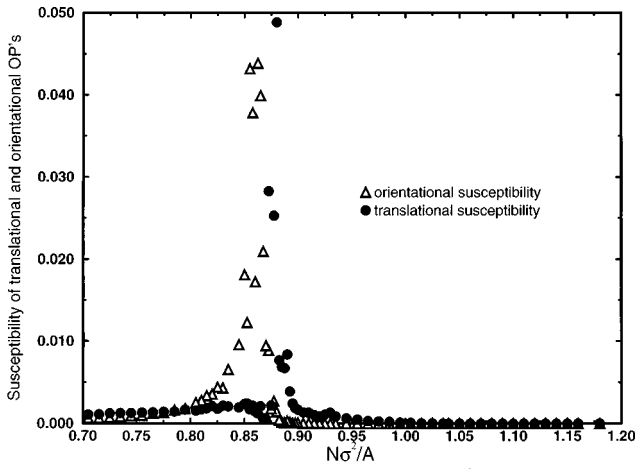

FIG. 8. The susceptibility of the translational (filled circles) and orientation (empty triangles) order parameters as a function of the 2D density.

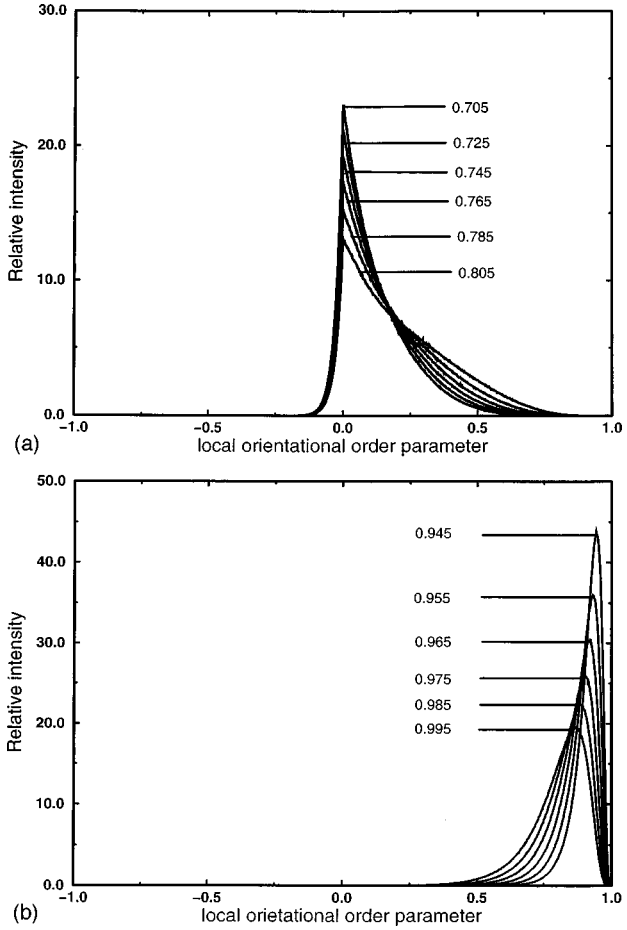

FIG. 9. The local orientation order parameter distribution for several 2D densities: (a) 0.705–0.805, representing the liquid phase. (b) 0.945–0.995, representing the solid phase.

of the liquid, hexatic, and solid phases identified above, for the system with the full Marcus-Rice potential, are listed in Table I.

The results of the Bladon-Frenkel analysis of the phase diagram of a two-dimensional assembly of disks which interact via a pairwise additive potential consisting of a hard core repulsion and a very narrow square well attraction (or a

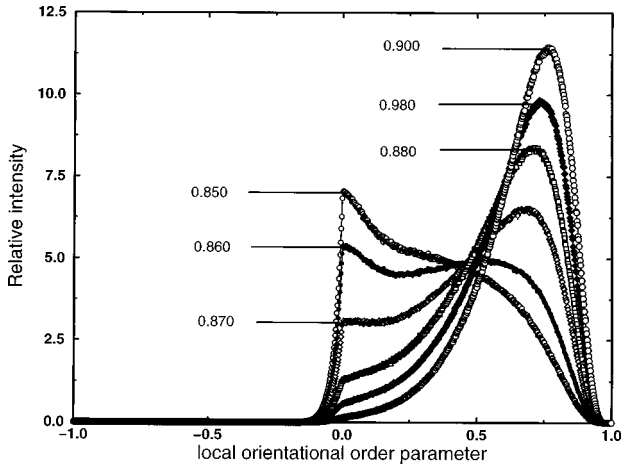

FIG. 10. The local orientation order parameter distribution inside the van der Waals loop, for the 2D densities 0.850–0.900.

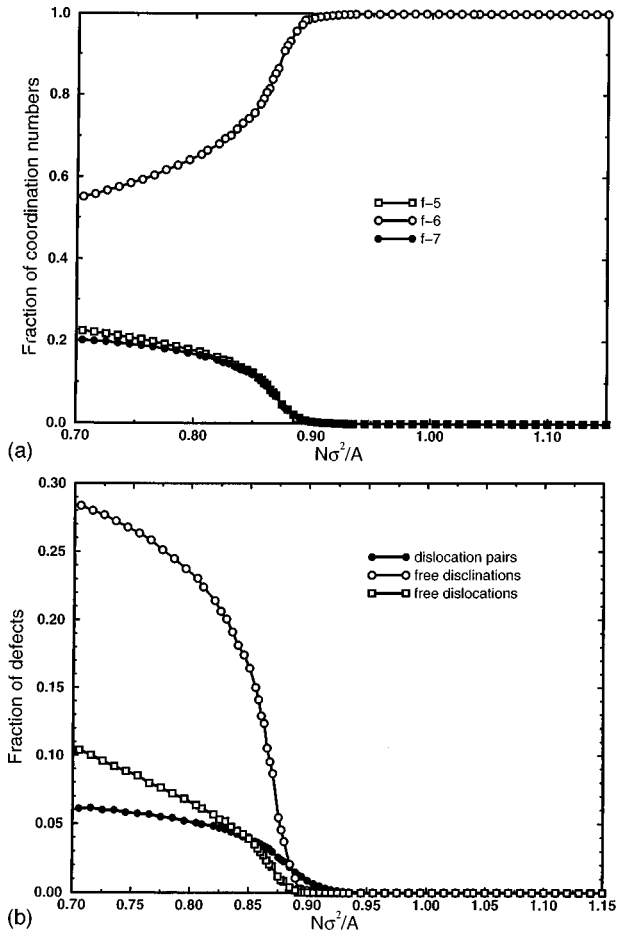

FIG. 11. (a) The fraction of particles which has 5 (empty squares), 6 (empty circles), and 7 (filled circles) as coordination numbers as a function of the 2D density. (b) Fraction of dislocation pairs (filled circles), free dislocations (empty squares), and free disclinations (empty circles) as a function of the 2D density.

very narrow step repulsion) are very sensitive to the width of the attractive well (or the step repulsion), because the system supports an isostructural solid-solid phase transition only when that width is small relative to the disk diameter. To examine the influence of the attractive well of the Marcus-Rice potential on the phase diagram of the quasi-two-dimensional system, we carried out simulations in which that part of the interparticle potential is deleted. The resulting potential is everywhere repulsive and, for the region $1.00 \leqslant r^* \leqslant 1.04$, rather soft. Consequently, it is not obvious that the system with modified Marcus-Rice interactions can support an isostructural solid-solid transition and a hexatic phase.

TABLE I. The phase boundaries for the Marcus-Rice potential and for the modified Marcus-Rice potential, for $T^* = 1.0$ and $H = 1.2\sigma$.

	2D density	
Phase	Marcus-Rice potential	Modified Marcus-Rice potential
Solid	0.900	0.890
Hexatic	0.880–0.870	0.870–0.860
Liquid	0.850	0.840

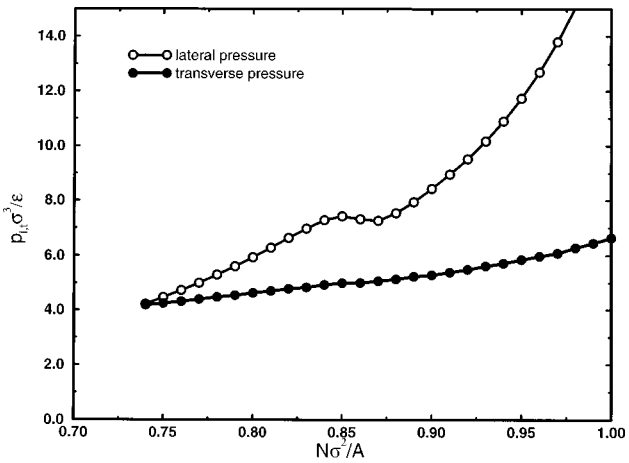

FIG. 12. Lateral pressure (empty circles) and transverse pressure (filled circles) isotherms as a function of the 2D density for the modified Marcus-Rice potential.

We show in Fig. 12, for the $T^* = 1.0$ isotherm, the lateral and transverse pressures versus density for the range $0.740 \leqslant \rho^* \leqslant 1.000$. As in the system with the full Marcus-Rice potential, there is a van der Waals loop in the lateral pressure (while the transverse pressure is continuous), indicating that the system supports a first order phase transition that occurs in the plane. Note that in the absence of the attractive well the van der Waals loop is shifted to the slightly lower density range $0.840 \leqslant \rho^* \leqslant 0.890$. In this system both the constant volume heat capacity $c_{A,H}$ (Fig. 13) and the thermal lateral and transverse pressure coefficients (Fig. 14) have a sharp peak at $\rho^* = 1.150$, but nowhere else in the density range studied. As in the system with the full Marcus-Rice potential, the global translational and orientational order parameters become zero at different densities (Fig. 15), at which their corresponding susceptibilities are singular (Fig. 16). The densities of the liquid, hexatic, and solid phases in the system with the modified Marcus-Rice potential are listed in Table I.

B. Transitions in the solid phase: Small lattice distortions and buckling

We now examine the distribution of lattice spacings (the analysis is in three dimensions) for the density range

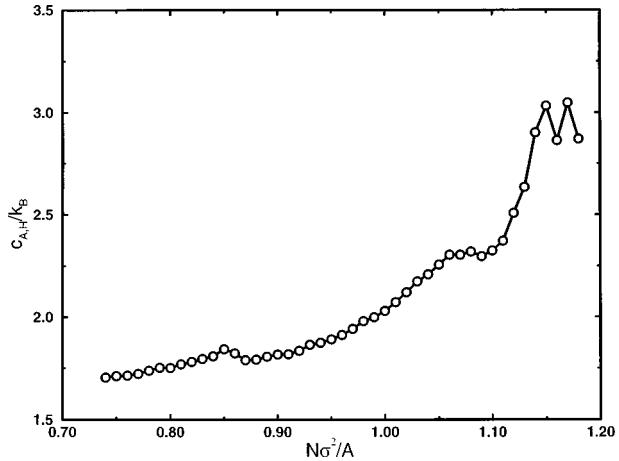

FIG. 13. Heat capacity at constant A and H as a function of the 2D density for the modified Marcus-Rice potential.

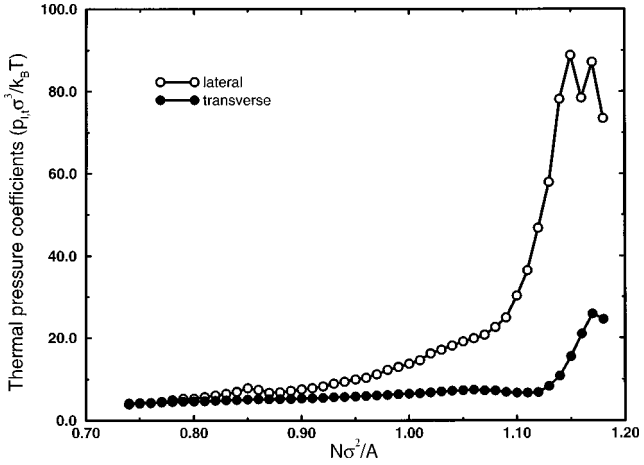

FIG. 14. Lateral (empty circles) and transverse (filled circles) thermal pressure coefficients as a function of the 2D density for the modified Marcus-Rice potential.

$1.050 \leqslant \rho^* \leqslant 1.140$ (Fig. 17) and the distributions of lattice spacings in the density ranges $0.945 \leqslant \rho^* \leqslant 1.040$ [Fig. 18(a)] and $1.150 \leqslant \rho^* \leqslant 1.180$ [Fig. 18(b)]. The latter two distributions are unimodal, whereas that for $1.050 \leqslant \rho^* \leqslant 1.140$ is bimodal. We find that the distribution of the local orientational order parameter in the coexistence region is unimodal and very narrow, with a peak value of 1.00, and that the global translational and orientational order parameters in the coexistence region have values in the ranges 0.983–0.993 and 0.990–0.996, respectively. Analysis of the distribution of the absolute orientations of the Voronoi polygons (displayed in Fig. 19) reveals that it is very narrow and unimodal. We infer that the structural transition we have observed affects only the magnitude of the nearest neighbor separation i.e., the two phases have the same orientation with respect to a space fixed axis. In one phase the value of the nearest neighbor separation is centered at the minimum of the Marcus-Rice potential, whereas in the other phase the nearest neighbor separation varies in the range $1.010 \leqslant r^* \leqslant 1.035$ as the two-dimensional density increases. Note that $1.010 \leqslant r^* \leqslant 1.035$ is just the range of r^* which corresponds to the slowly varying part of the repulsive component of the Marcus-Rice potential.

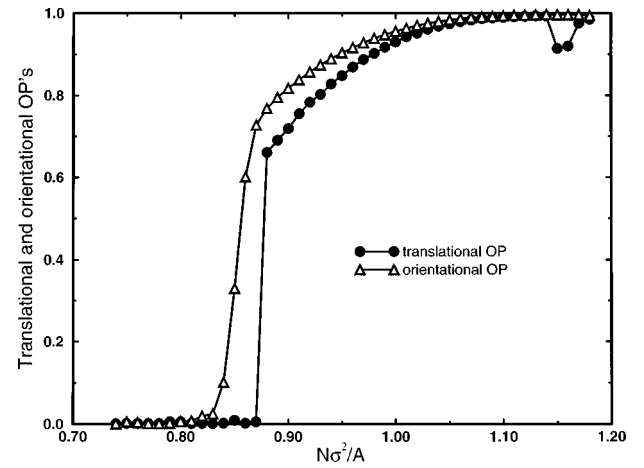

FIG. 15. The global translational (filled circles) and orientational (empty triangles) order parameters as a function of the 2D density for the modified Marcus-Rice potential.

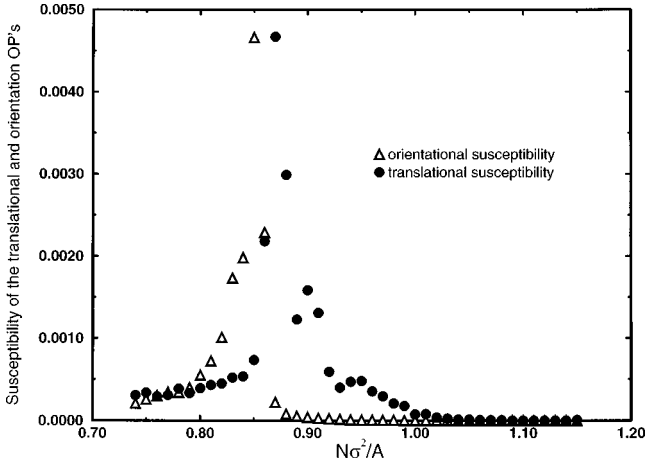

FIG. 16. The susceptibility of the translational (filled circles) and orientational (empty triangles) order parameters as a function of the 2D density for the modified Marcus-Rice potential.

Although the preceding observations suggest the occurrence of a first order isostructural phase transition between two solid phases, each of which has triangular lattice symmetry, a different picture emerges when we examine the configurations of the two ''phases'' projected on the *xy* plane (Fig. 20). This projection clearly shows that the long and short lattice spacings are not ordered, and that no phase separation has occurred. To verify that the configuration displayed is not that for a system trapped in a local minimum, we have carried out a simulation for $\rho^* = 1.090$ starting with a configuration that has separated phases. Specifically, in this initial configuration the ''high'' and ''low density'' solid phases occupied different regions, with the particles placed at a height *z* that corresponds to the maximum of the height distribution at $\rho^* = 1.090$ with an ordered linear buckled structure. The simulations were carried out twice, once with time step equal to 5×10^{-4} and once with time step equal to 1×10^{-5}. In both cases the final configuration after 10×10^6 cycles was a single phase with a disordered distribu-

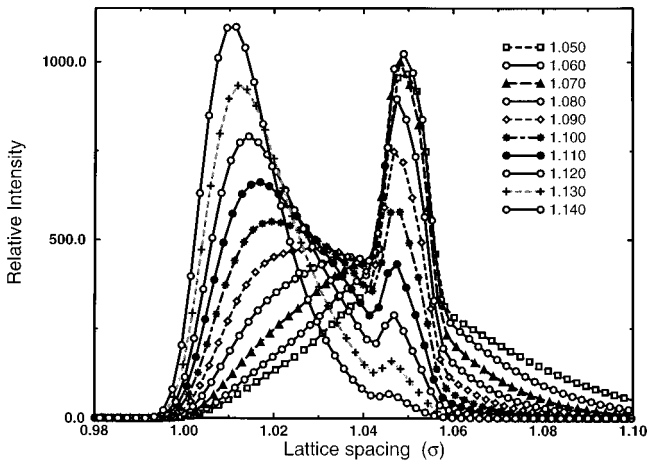

FIG. 17. The lattice spacing distribution for 2D densities 1.050–1.140 (shown with equal intervals). $\rho^* = 1.050$ is the distribution that has the dominant peak at the lattice spacing that corresponds to the minimum in the Marcus-Rice potential (1.05), while $\rho^* = 1.140$ has the major peak around a lattice spacing of 1.01.

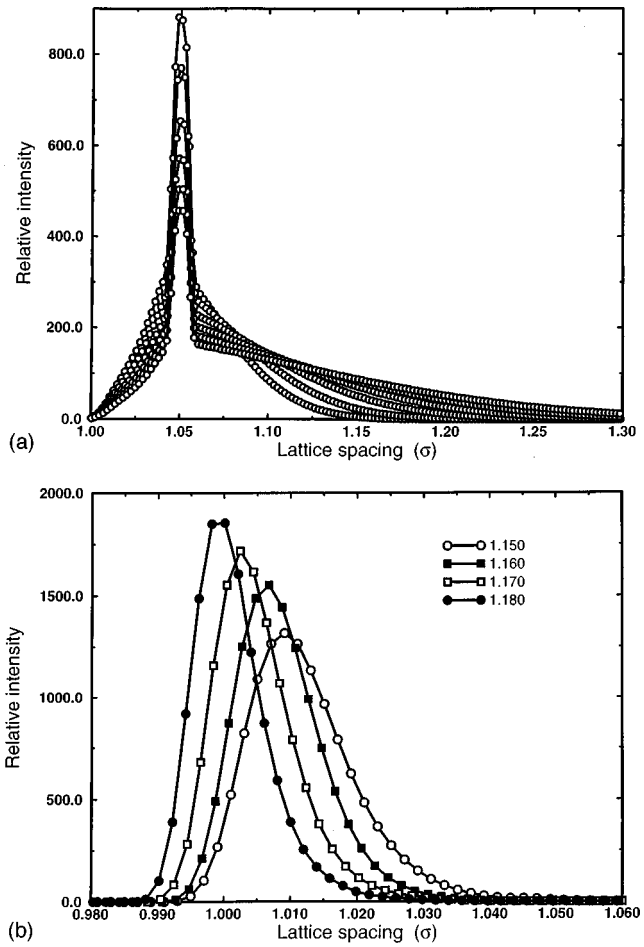

FIG. 18. The lattice spacing distribution for 2D densities: (a) 0.945–1.040. (b) 1.150 (empty circles), 1.160 (filled squares), 1.170 (empty squares), and 1.180 (filled circles).

tion of the two different lattice spacings. Indeed, this conclusion is consistent with Landau theory (notwithstanding the questionable applicability of that theory to two dimensional systems) and the character of the isotherms for our model system. Landau theory predicts that coexisting phases with the same symmetry are connected by a first order transition; hence there should be a plateau in the pressure-density isotherm for the coexistence region. Our simulation results reveal a plateau in neither the lateral nor transverse pressure-density isotherms in the range for which the behavior described above exists (see Fig. 21). Moreover, we find that the constant volume heat capacity $C_{A,H}$ (Fig. 3) and the lateral thermal pressure coefficients (Fig. 4) of the model system with the full Marcus-Rice potential exhibit singularities near $\rho^* = 1.050$, and that the energy per particle distribution is unimodal (Fig. 22) for the density range associated with the transition. Taken together, these observations suggest the occurrence of a continuous phase transition between the identified solid phases.

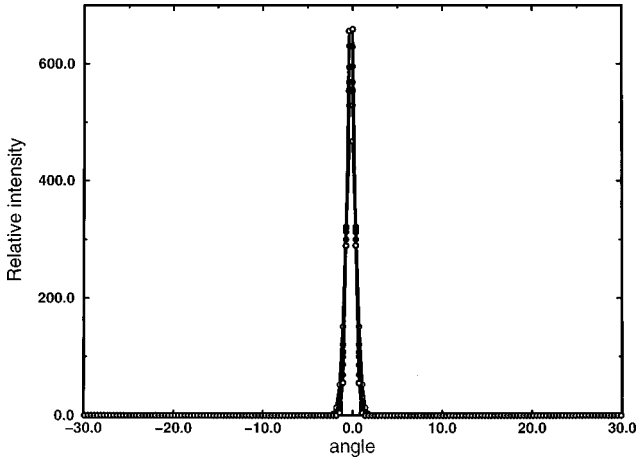

FIG. 19. The orientation of the Voronoi polygons for 2D densities 1.050–1.140, as defined in Eq. (2.13).

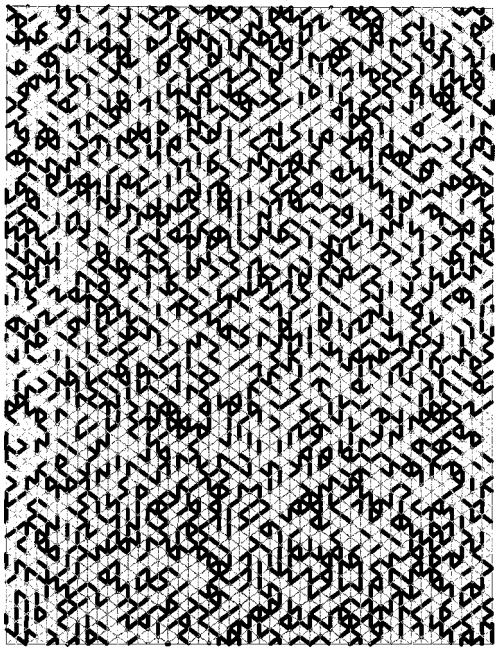

FIG. 20. Lateral arrangement of the short (gray lines) and long (black lines) lattice spacings for the 2D density 1.090.

Given that there are two configurations of the particles with different average nearest neighbor spacings, why is there not a separation of the assembly of particles into two distinct phases? We attempt to answer this question by noting that, taking advantage of the short range of the interaction between particles, the potential energy of our model system can be represented in the form

$$\mathcal{U} = \tfrac{1}{2}\sum_{i=1}^{N}\sum_{j}^{n_i} u(r_{ij}) + \sum_{i=1}^{N} u_{\mathrm{ext}}(z_i), \tag{3.1}$$

where the second sum of the first term goes over only the nearest neighbors of particle i. Since the particles in the system form a single sheet the nearest neighbor connectivity is two dimensional, even if that sheet crumples. Then, for a specified distribution of number of nearest neighbor spacings, the potential energy of the model system is the same whether the particles are partitioned into aggregates which are homogeneous with respect to nearest neighbor spacing or are thoroughly mixed with respect to nearest neighbor spacing. Accordingly, with the stated constraint, the spatial arrangement of nearest neighbor separations will be determined by maximizing the entropy of that arrangement.

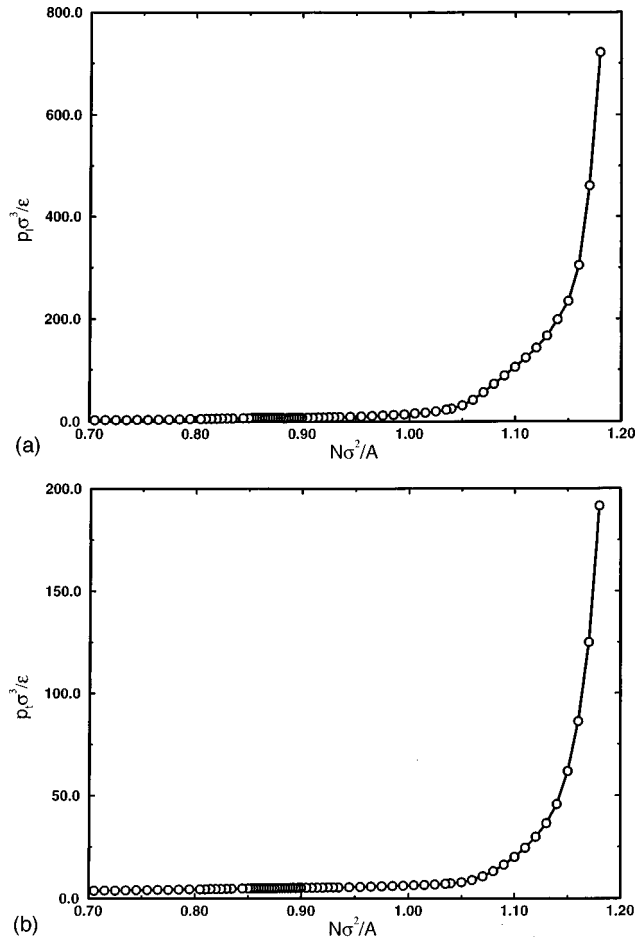

FIG. 21. Lateral pressure (a) and transverse pressure (b) as a function of the 2D density for the full Marcus-Rice potential.

When we carried out the simulation without the attractive part of the interparticle potential, the distribution of the lattice spacing was unimodal for all the densities that correspond to the solid phase. Moreover, in this case neither the heat capacity $c_{A,H}$ (Fig. 13) nor the thermal pressure coefficients (Fig. 14) exhibit any singularities aside from those corresponding to the buckling transition, indicating that there was no distortion of the triangular lattice.

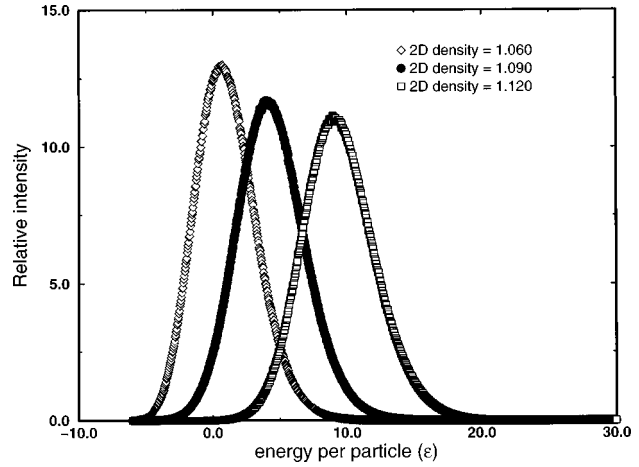

FIG. 22. Distribution of the total energy (kinetic plus potential) of the particles for the 2D densities 1.060 (empty diamonds), 1.090 (filled circles), and 1.120 (empty squares).

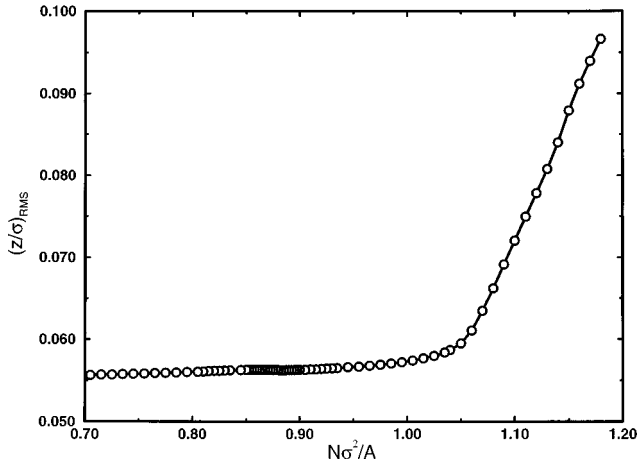

FIG. 23. Root mean square of the displacement of the z coordinate from the midplane of the cell as a function of the 2D density.

At the same density at which the distortion of the triangular lattice which we associate with the structural transition begins, the particles begin to be displaced from the midplane $z^*=0$, and there is a marked increase in $(\partial p/\partial\rho)_T$. The former feature is evident in the dependence of the root mean square displacement of the particles from $z^*=0$ (Fig. 23). In Fig. 24 we show the density profile along the z axis for several average system densities in the range $1.040 \leqslant \rho^* \leqslant 1.180$. When $\rho^* \leqslant 1.040$ that density profile is sensibly uniform, there is only one phase present in the cell and the symmetry of the packing in the xy plane is hexagonal. At very high average system densities, $\rho \geqslant 1.140$, the density profile along the z axis has peaks adjacent to the walls of the cell, and there is only one out of plane phase. For densities in the range $1.050 \leqslant \rho^* \leqslant 1.140$ there is a continuous transition between those two limiting situations with both components present at all intermediate densities.

It is interesting that the onset of the triangular distortions begins with out of plane motion and finishes with the transition to the ordered buckled phase. That transition occurs near $\rho^*=1.150$, at which density the constant volume heat capacity $c_{A,H}$ (Fig. 3) and the lateral and transverse thermal pres-

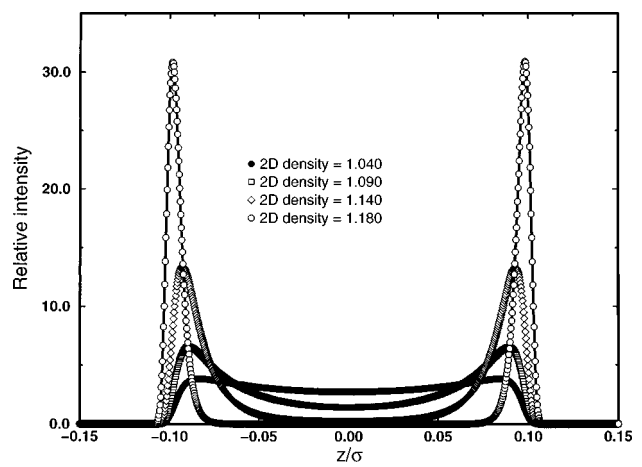

FIG. 24. The density distribution as a function of the height in the cell for 2D densities 1.040 (filled circles), 1.090 (empty squares), 1.140 (empty diamonds), and 1.180 (empty circles).

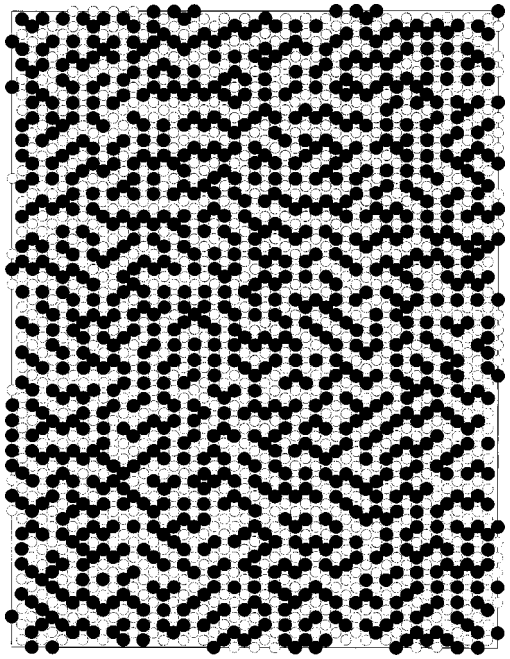

FIG. 25. Lateral configuration of up ($z>0$, filled circles) and down ($z<0$, empty circles) particles for the 2D density 1.140.

sure coefficients (Fig. 4) show singularities. However, the lateral and transverse pressure-density isotherms are continuous (see Fig. 21), signalling again the occurrence of a continuous phase transition. Clearly, the system has undergone a transition from a quasi-two-dimensional hexagonal solid to a buckled solid. This buckling transition was observed in both of the systems studied, i.e., with the full Marcus-Rice potential and with the modified Marcus-Rice potential. Figures 25 and 26 display the lateral structure of the buckled phase for $\rho^*=1.140$ and 1.160, respectively, for the system with the Marcus-Rice potential. The figures show that when ρ^*

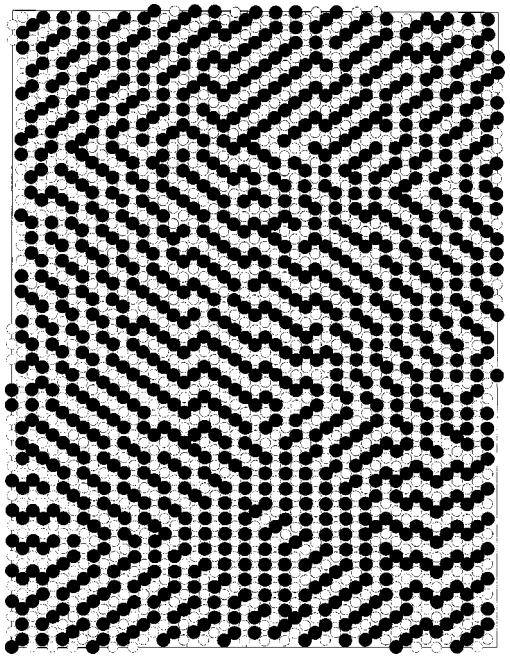

FIG. 26. Lateral configuration of up ($z>0$, filled circles) and down ($z<0$, empty circle) particles for the 2D density 1.160.

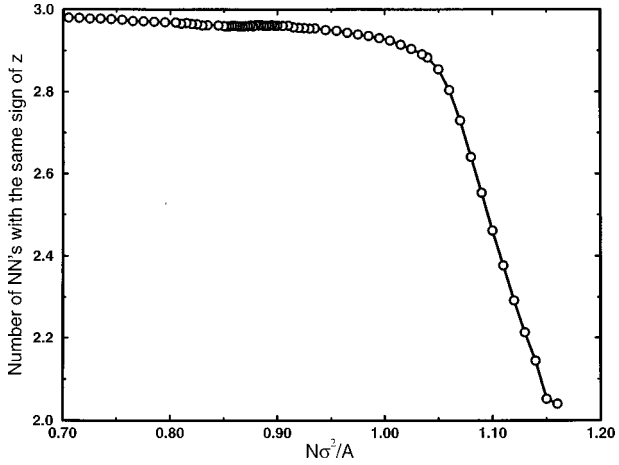

FIG. 27. The number of nearest neighbors with the same sign of the height (z) coordinate as a function of the 2D density.

$=1.140$ there are small regions of linear and zigzag buckling, but they are not ordered with respect to each other, whereas when $\rho^*=1.160$ there is an ordered phase of linear and zigzag buckling that has a broken symmetry with respect to twofold rotation. As already mentioned, the nearest neighbor connectivity is two dimensional even when the particles are in the buckled phase, so one can still construct the Voronoi polygon in two dimensions to determine the number of nearest neighbors (NNs). This number is six for all the particles in the high density region, but as the particles start to move out of the plane, one can count how many of those nearest neighbors move with this particle in the same direction. An uncorrelated configuration is generated when half of the nearest neighbors move with the tagged particle, while complete correlation is generated when there are just two nearest neighbors, thereby forming linear or zigzag buckling. In Fig. 27 we show the average number of nearest neighbors to a particle, all with the same value of z^*, as a function of the two-dimensional density. We notice that when $\rho^*=1.040$ there are close to three nearest neighbors per particle, as expected for a planar configuration of the particles (where there is no correlation in the z coordinate of the NN particles). However, as ρ^* is increased above this density, the number of nearest neighbors per particle decreases continuously to two indicating that the onset of the ordered buckling transition starts with the lattice distortion and the out of plane motion, but cannot proceed far because some of the particles are still in the plane. We have monitored the interplay between the triangular distortion and the buckling as a function of the sample thickness H by carrying out simulations at the constant density $\rho^*=1.150$. We find that when H increases sufficiently the ordered buckled triangular lattice melts, but that ordered buckling is sustained all the way to melting. Moreover, the distortion of the triangular lattice occurs with the buckled phase present. After melting the separation of the system into two layers persists, and a bilayer, separated by a small diffusive region, is formed when $H>2$. We thereby infer that a necessary condition for ordered buckling to occur is formation of a complete out of plane arrangement. We also conclude that as H increases the ordered buckling transition will occur at lower densities, i.e., the excess free energy for attaining the out of plane configuration decreases, and there is a point (a triple point) at which

the in plane triangular lattice becomes unstable with respect to the buckled phase just as is the case for hard spheres between smooth hard walls [39].

We note that for both the Marcus-Rice and modified Marcus-Rice potentials the global translational order parameter exhibits a small minimum at $\rho^*=1.150$, which we interpret as arising from the occupation of the particles of the free volume that is accessible to them. At lower densities, the particles are fully or partially in the midplane, and for all values of z the projected triangular symmetry on the midplane is preserved. When buckling occurs, the particles have less space to move in the vertical direction but the accessible lateral volume (above the mid plane of the cell for particles with $z>0$, and below for particles with $z<0$) is increased, so the projected triangular symmetry can then accept small distortions, and even rows of up and down particles can move slightly with respect to one another. This increase in lateral accessible volume will be a maximum for the lowest two-dimensional (2D) density that supports ordered buckling; in our case that corresponds to the density $\rho^*=1.150$.

IV. DISCUSSION

The simulation studies reported in this paper were undertaken to test the inference that a quasi-two-dimensional system of particles with Marcus-Rice-type pair interactions will support first order liquid-to-hexatic and hexatic-to-solid phase transitions. Our results show that this inference is correct; for the isotherm with $T^*=1$, these phase transitions occur sequentially as the density is increased from $\rho^*=0.850$ to 0.900. On the other hand, the inference which follows from the work of Bladon and Frenkel and Chou and Nelson, that the existence of the first order liquid-to-hexatic and hexatic-to-solid transitions is coupled to the existence of a first order isostructural solid-to-solid transition, is found not to hold. A model system in which there are Marcus-Rice-type pair interactions does support a solid-to-solid isostructural transition in the density range $1.050\leqslant\rho^*\leqslant1.140$, but that transition is found to be continuous. Moreover, a model system in which there are modified Marcus-Rice-type pair interactions, without any attractive component, exhibits first order liquid-to-hexatic and hexatic-to-solid transitions in the density range $0.840\leqslant\rho^*\leqslant0.890$ even though that system does not support a solid-to-solid isostructural transition. Finally, we have observed that both model systems studied, with and without an attractive component in the pair interaction, support a buckling transition when the density is greater than $\rho^*=1.150$.

We now examine some of the features of the structural changes associated with the observed structural transitions. We consider, first, the high density buckling transition. A transition of this type has been shown to occur in a system of hard spheres confined between parallel plates [39]. The information concerning the system of hard spheres confined between parallel plates which is pertinent to us is for the domain in which the separation between the plates is in the range $\sigma<H<1.57\sigma$. In this domain the low density stable phase is the liquid. For any fixed value of H, as the density is increased the liquid undergoes a first order transition to a hexagonal two-dimensional solid. Further increase in the density generates a first order transition from the hexagonal solid to an ordered buckled solid phase; the latter phase is stable up to close packing. As H is decreased below about 1.5σ, the densities at which the liquid-to-hexagonal solid and the hexagonal solid-to-buckled solid transitions occur increase, and the hexagonal solid-to-buckled solid transition vanishes when $H=\sigma$. When the plate separation is $H=1.2\sigma$, which is the value appropriate for comparison with our simulations, the difference in densities of the unbuckled and buckled phases is very small. As H is increased from the lower to the upper end of the range $\sigma<H<1.57\sigma$, the density interval in which the buckled solid phase is stable grows at the expense of that of the two-dimensional hexagonal solid phase, up to $H=1.57\sigma$, where there is a triple point between the fluid, hexagonal two-dimensional solid and buckled solid phases. For larger values of H, the hexagonal two-dimensional solid phase is unstable.

As already noted, our simulations correspond to $H=1.2\sigma$. For this value of H the hexagonal solid-to-buckled solid transition in the hard sphere system occurs at $\rho^*=1.17$, very close to the value $\rho^*=1.150$ for the system with the Marcus-Rice potential and the modified Marcus-Rice potential. If the density difference between the unbuckled and buckled phases for a system with the Marcus-Rice potential is as small as it is for a hard sphere system, the combined effects of statistical error and density interval sampling in our simulations is likely sufficient to mask the first order character of the transition between these phases.

We now consider the isostructural solid-to-solid transition in the system with the Marcus-Rice potential. The unusual feature associated with this transition is that, in the coexistence region, the low density phase has a fixed lattice spacing but the high density phase has a lattice spacing that decreases continuously with increasing density. We note that the particle spacing in the low density phase corresponds to the minimum in the Marcus-Rice potential, and the density dependent particle spacings in the high density phase correspond to points on the softly repulsive part of the Marcus-Rice potential. In a conventional first order transition, the average density in the coexistence region fixes the amounts of each phase since the densities of these phases are not dependent on the average density (the lever rule). In our case, in the coexistence region the phase with particle spacing equal to the minimum in the Marcus-Rice potential has a fixed density, and the remainder of the space is taken up by the other, higher density, phase. The two phases are isostructural both because there is insufficient room for rearrangement of the particles, and because hexagonal packing is the most efficient of all possible particle packings in the plane.

We interpret the observation that the particle spacing in the higher density phase adjusts to accomodate to the space available as follows. The Marcus-Rice potential, although everywhere continuous, has a relatively sharp ''corner'' where the soft repulsion merges with the attractive well. A similar corner exists in the model potential which has a hard core plus a narrow finite height step repulsion. For the latter, it is known that when the width of the step repulsion is small compared to the hard core diameter, the potential supports an isostructural solid-to-solid transition [40,14]. We expect the corner in the Marcus-Rice potential to play a similar role in cleanly separating the potential energy surfaces of the high and low density phases. It is plausible that the higher density

solid supported by the Marcus-Rice potential will be very much more compressible than the low density solid because of the difference between the responses to displacement along the soft repulsion in the range $\sigma \leqslant r^* \leqslant 1.04\sigma$ and displacement in the potential well in the range $1.04\sigma \leqslant r^* \leqslant 1.06\sigma$.

Arguably the most interesting inference which can be drawn from our simulation results concerns the influence of motion in the z direction on the character of the isostructural solid-to-solid phase transition. Although both the strictly two-dimensional simulation studies of Bladon and Frenkel and the analytical theory of Chou and Nelson appear to account for the phase transitions we find in the density range $0 < \rho^* \leqslant 1.140$, the fact that the associated isostructural solid-to-solid transition is required to be first order is not in agreement with our results. Moreover, we find that the continuous isostructural phase transition in the density range $1.050 \leqslant \rho^* \leqslant 1.140$ involves displacement of the particles in the z direction, and that the isostructural character of the transition is achieved because the projection of the positions of the particles with $z \neq 0$ on the median plane retains the triangular symmetry of the low density phase. Then the predicted behavior of a strictly two-dimensional system is retained in a quasi-two-dimensional system via exploitation of motion in the z direction. An analogous situation occurs in the analysis of the phase diagram of Langmuir monolayers, modeled as rods attached at one end to the water surface. Kaganer and co-workers [41] showed that a strictly two-dimensional Landau theory analysis of the Langmuir monolayer phase diagram, based on the assumption that one-dimensional crystallization in the monolayer is stable so that order parameters can be assigned for that crystallization in the x and y directions, accurately reproduces all the characteristic features observed. However, one dimensional crystallization is absolutely unstable in two dimensions, but is stable in three dimensions. Since a number of the phases of a dense Langmuir monolayer differ by virtue of the tilt of the rodlike molecules relative to the normal to the surface, changes of phase necessarily involve some motion by the molecules in the z direction, with the projections of the molecules on the xy plane constrained to satisfy the packing symmetries of the phases. As in the study reported in this paper, exploitation of motion in the z direction preserves the essential character of the predicted two-dimensional behavior. We suspect that in the real three-dimensional world, where realizations of two-dimensional systems always involve some coupling with the third dimension, the behavior we have found will be common.

ACKNOWLEDGMENTS

The research reported in this paper was supported by the National Science Foundation via Grant No. NSF CHE-9528923, with assistance from the Materials Research Science and Engineering Center at The University of Chicago, supported by the NSF under Grant No. DMR-9400379.

APPENDIX: PRESSURES AND THERMAL PRESSURE COEFFICIENTS

The existence of an external field along the z axis, whether symmetric about $z = 0$ as in our case, or asymmetric, implies that all of the thermodynamic properties of the system are functions of the strength of the external field. Suppose the system is contained in a rectangular box. If N, T, and V are held constant, the field strength determines the area in the xy plane, A, and the height in the z direction, H. Alternatively, one can work with the variables A and H instead of the volume and the field strength. Moreover, in the presence of an external field along the z axis we must consider separately the variation of the thermodynamic properties of the system parallel to z (the transverse component) and in the xy plane (the lateral component). We note, as an exception to the preceding statement, that the heat capacity at constant volume and field strength does not have different transverse and lateral values since it is equivalent to $c_{A,H}$. We also note that because the thermodynamic potentials of the system depend on the strength of the external field, which represents an extra degree of freedom, the Gibbs phase rule assumes the form

$$f = 3 - p + c, \tag{A1}$$

where f is the number of degrees of freedom, p is the number of phases, and c is the number of components. Then, in a one component system, there can be a point where four phases coexist, a line of a coexistance between three phases, etc.

1. Lateral and transverse pressures

The expressions for the lateral and transverse pressures can be derived either from mechanics or from thermodynamics. The mechanical treatment was introduced by Clausius for homogenous systems [42]. Consider the equations of motion in the xy plane of a particle with mass m and with center of mass coordinates x and y, subject to a force whose components are $\mathcal{F}_x$ and $\mathcal{F}_y$:

$$m \frac{d^2x}{dt^2} = \mathcal{F}_x, \tag{A2a}$$

$$m \frac{d^2y}{dt^2} = \mathcal{F}_y. \tag{A2b}$$

Multiplying Eq. (A2a) by $\frac{1}{2}x$, Eq. (A2b) by $\frac{1}{2}y$, and summing over all the N particles in the system, yields

$$\frac{1}{4}\sum_{i=1}^{N} \frac{d^2}{dt^2}[m(x_i^2 + y_i^2)] = \frac{1}{2} m \sum_{i=1}^{N} (v_{x_i}^2 + v_{y_i}^2) + \frac{1}{2}\sum_{i=1}^{N} (\mathcal{F}_{x_i} x_i + \mathcal{F}_{y_i} y_i), \tag{A3}$$

where v_x and v_y are the components of the velocity vector in the x and y directions. Note that this equation describes the motions of the N particles in the xy plane for all values of z. Integration over time from 0 to τ yields

$$\frac{1}{4}\left[\frac{d}{dt}\sum_{i=1}^{N} m(x_i^2+y_i^2)\right]_0^{\tau} = \tau\,\frac{1}{2}\,m\left\langle\sum_{i=1}^{N}(v_{x_i}^2+v_{y_i}^2)\right\rangle + \tau\,\frac{1}{2}\left\langle\sum_{i=1}^{N}(\mathcal{F}_{x_i}x_i+\mathcal{F}_{y_i}y_i)\right\rangle. \tag{A4}$$

For a system in equilibrium, the left hand side of this equation is zero. The second term on the right hand side is the lateral virial with a negative sign, which can be written in terms of internal forces (between the molecules) and external forces (stresses across the boundaries of the system). The stress per unit area is the lateral pressure. If dS is a surface element of the lateral boundary surface Σ_l, and n_x and n_y are the directions of the outward normals in the x and y directions, the contribution of the external forces to the virial is $\frac{1}{2}p_l\int\int_{\Sigma_l}(n_x x+n_y y)dS$. Using Green's theorem, this surface integral can be rewritten as a triple integral over the volume of the system, and we need to evaluate the stress along the entire height H. The internal virial can be expressed as the sum over pairs of particles of the radial derivative of the interparticle potential,

$$\frac{1}{2}\sum_{i=1}^{N}(\mathcal{F}_{x_i}x_i+\mathcal{F}_{y_i}y_i) = -\frac{1}{2}\,p_l\int\int\int_V\left(\frac{\partial x}{\partial x}+\frac{\partial y}{\partial y}\right)dV - \frac{1}{2}\sum_{i=1}^{N}\sum_{j>i}^{N}\left.\frac{x_{ij}^2+y_{ij}^2}{r_{ij}}\frac{\partial u(r)}{\partial r}\right|_{r=r_{ij}} \tag{A5}$$

$$= -p_l V+\mathcal{W}_l, \tag{A6}$$

where $\mathcal{W}_l$ is the internal lateral virial. From the equipartition theorem in the thermodynamic limit ($N\to\infty$), $\frac{1}{2}m\Sigma_{i=1}^{N}(v_{x_i}^2+v_{y_i}^2)=Nk_BT$, which leads to the following expression for the lateral pressure:

$$p_l V=Nk_BT+\langle\mathcal{W}_l\rangle. \tag{A7}$$

The calculation of the transverse pressure follows the same procedure. We find that

$$\frac{1}{2}\,m\left\langle\sum_{i=1}^{N}v_{z_i}^2\right\rangle = -\frac{1}{2}\left\langle\sum_{i=1}^{N}(\mathcal{F}_{z_i}z_i)\right\rangle. \tag{A8}$$

The transverse virial also has internal force and external force contributions. The transverse boundary surface is $\Sigma_t=2A$, but since in our model system there is no periodic boundary condition in the z direction, nor is it the case that the particle diameter is much smaller than H, the transformation to a volume integral yields $V'=Ah$. We then find, for the transverse pressure,

$$p_t V'=Nk_BT+2\langle\mathcal{W}_t\rangle, \tag{A9}$$

where the internal transverse virial is

$$\mathcal{W}_t=-\frac{1}{2}\sum_{i=1}^{N}\sum_{j>i}^{N}\left.\frac{z_{ij}^2}{r_{ij}}\frac{\partial u(r)}{\partial r}\right|_{r=r_{ij}}. \tag{A10}$$

The transverse pressure can be calculated in a more direct form since we know the external field in the z direction,

$$p_t=\frac{1}{V'}\sum_{i=1}^{N} z_i\left.\frac{\partial u_{ext}(z)}{\partial z}\right|_{z=z_i}=\frac{1}{2A}\sum_{i=1}^{N}\left.\frac{\partial u_{\rm ext}(z)}{\partial z}\right|_{z=|z_i|}. \tag{A11}$$

Combining the expressions for the lateral pressure and the transverse pressure [Eq. (A9)], and letting $p_l=p_t=p$ and $h\to H$, we recover the homogeneous case pressure

$$pV=Nk_BT+\tfrac{2}{3}\langle\mathcal{W}\rangle. \tag{A12}$$

The internal virial $\mathcal{W}$ is $\mathcal{W}=\mathcal{W}_l+\mathcal{W}_t=-\frac{1}{2}\Sigma_{i=1}^{N}\Sigma_{j>i}^{N}r_{ij}[\partial u(r)/\partial r]|_{r=r_{ij}}$. Setting $H=1$ ($h=0$) so that $V=A$ in Eq. (A7) gives the pressure in two dimensions, which has units of force per unit length, whereas the transverse pressure (A9) goes to infinity.

2. Thermal pressure coefficients

Expressions for the thermal pressure coefficients can be obtained by differentiation of Eqs. (A7) and (A9) with respect to the temperature at constant A and H. If we use the canonical ensemble, then those quantities can be calculated from the cross correlation between the fluctuations in the potential energy and the corresponding virials:

$$\left(\frac{\partial\langle\mathcal{W}_l\rangle}{\partial T}\right)_{A,H,N}=\frac{1}{k_BT^2}\,\langle\delta\mathcal{W}_l\delta\mathcal{U}\rangle, \tag{A13a}$$

$$\left(\frac{\partial\langle\mathcal{W}_t\rangle}{\partial T}\right)_{A,H,N}=\frac{1}{k_BT^2}\,\langle\delta\mathcal{W}_t\delta\mathcal{U}\rangle. \tag{A13b}$$

For the canonical ensemble, we find

$$\left(\frac{\partial p_l}{\partial T}\right)_{A,H}\equiv\gamma_l=\frac{1}{V}\left(Nk_B+\frac{\langle\delta\mathcal{U}\delta\mathcal{W}_l\rangle}{k_BT^2}\right), \tag{A14a}$$

$$\left(\frac{\partial p_t}{\partial T}\right)_{A,H}\equiv\gamma_t=\frac{1}{V'}\left(Nk_B+\frac{2\langle\delta\mathcal{U}\delta\mathcal{W}_t\rangle}{k_BT^2}\right). \tag{A14b}$$

We now use the transformation of fluctuations between ensembles derived in Ref. [38] to rewrite these expressions for the microcanonical ensemble:

$$\gamma_l=\frac{1}{V}\left(Nk_B+\frac{2c_{A,H}\langle\delta\mathcal{U}\delta\mathcal{W}_l\rangle}{3k_B^2T^2}\right), \tag{A15a}$$

$$\gamma_t=\frac{1}{V'}\left(Nk_B+\frac{4c_{A,H}\langle\delta\mathcal{U}\delta\mathcal{W}_t\rangle}{3k_B^2T^2}\right). \tag{A15b}$$

[1] F. Bloch, Z. Phys. **61**, 206 (1930).
[2] R. Peierls, Helv. Phys. Acta **7**, 81 (1934).
[3] R. Peierls, Ann. Inst. Henri Poincaré **5**, 177 (1935).
[4] R. Peierls, *Surprises in Theoretical Physics* (Princeton University Press, Princeton, 1979).
[5] L. D. Landau, Phys. Z. Sowjetunion **11**, 26 (1937).
[6] L. D. Landau and E. M. Lifshits, *Statistical Physics* (Pergamon, Oxford, 1986).
[7] N. D. Mermin, Phys. Rev. **176**, 250 (1968).
[8] J. M. Kosterlitz and D. J. Thouless, J. Phys. C **5**, L124 (1972); **6**, 1181 (1973).
[9] B. I. Halperin and D. R. Nelson, Phys. Rev. Lett. **41**, 121 (1978).
[10] D. R. Nelson and B. I. Halperin, Phys. Rev. B **19**, 2457 (1979).
[11] A. P. Young, Phys. Rev. B **19**, 1855 (1979).
[12] For a review, see D. R. Nelson in *Phase Transitions and Critical Phenomena*, edited by C. Domb and J. L. Lebowitz (Academic, London, 1983), Vol. 7.
[13] S. T. Chui, Phys. Rev. B **28**, 178 (1983).
[14] P. Bladon and D. Frenkel, Phys. Rev. Lett. **74**, 2519 (1995).
[15] T. Chou and D. R. Nelson, Phys. Rev. E **53**, 2560 (1996).
[16] K. J. Strandburg, Rev. Mod. Phys. **60**, 161 (1988).
[17] M. A. Stan and A. J. Dahm, Phys. Rev. B **40**, 8995 (1989).
[18] D. C. Glattli, E. Y. Andrei, and F. I. B. Williams, Phys. Rev. Lett. **60**, 420 (1988).
[19] H. W. Jiang and A. J. Dahm, Surf. Sci. **229**, 352 (1990).
[20] C. A. Murray and D. H. Van Winkle, Phys. Rev. Lett. **58**, 1200 (1988).
[21] C. A. Murray and R. A. Wenk, Phys. Rev. Lett. **62**, 1643 (1989).
[22] C. A. Murray, W. O. Sprenger, and R. A. Wenk, Phys. Rev. B **42**, 688 (1990).
[23] *Bond Orientational Order in Condensed Matter Systems*, edited by K. J. Strandburg (Springer-Verlag, New York, 1992).
[24] A. J. Armstrong, R. C. Mockler, and W. J. O'Sullivan, J. Phys.: Condens. Matter **1**, 1707 (1989).
[25] A. H. Marcus and S. A. Rice, Phys. Rev. E **55**, 637 (1997).
[26] M. A. Glaser and N. A. Clark, Adv. Chem. Phys. **83**, 543 (1993).
[27] H. Weber, D. Marx, and K. Binder, Phys. Rev. B **51**, 14 636 (1995).
[28] V. M. Bedanov, G. V. Gadiyak, and Y. E. Lozovik, Phys. Lett. **92A**, 400 (1982).
[29] V. M. Bedanov, G. V. Gadiyak, and Y. E. Lozovik, Zh. Eksp. Teor. Fiz. **88**, 1622 (1985) [Sov. Phys. JETP **61**, 967 (1985)].
[30] K. J. Naidoo and J. Schnitker, J. Chem. Phys. **100**, 3114 (1994).
[31] K. Bagchi, H. C. Andersen, and W. Swope, Phys. Rev. Lett. **76**, 255 (1996).
[32] W. C. Swope, H. C. Andersen, P. H. Berens, and K. R. Wilson, J. Chem. Phys. **76**, 637 (1982).
[33] L. Verlet, Phys. Rev. **159**, 98 (1967).
[34] M. P. Allen and D. J. Tildesley, *Computer Simulation of Liquids* (Clarendon, Oxford, 1989).
[35] F. P. Preparata and M. I. Shamos, *Computational Geometry, An Introduction* (Springer-Verlag, New York, 1985).
[36] B. Jancovici, Phys. Rev. Lett. **19**, 20 (1967).
[37] Y. Imry and L. Gunther, Phys. Rev. B **3**, 3939 (1971).
[38] J. L. Lebowitz, J. K. Percus, and L. Verlet, Phys. Rev. **153**, 250 (1967).
[39] M. Schmidt and H. Löwen, Phys. Rev. Lett. **76**, 4552 (1996); Phys. Rev. E **55**, 7228 (1997).
[40] P. Bolhuis and D. Frenkel, Phys. Rev. Lett. **72**, 2211 (1994); P. Bolhuis, M. Hagen, and D. Frenkel, Phys. Rev. E **50**, 4880 (1994).
[41] V. M. Kaganer and E. B. Loginov, Phys. Rev. E **51**, 2237 (1995); V. M. Kaganer, M. A. Osipov, and I. R. Peterson, J. Chem. Phys. **98**, 3513 (1993).
[42] R. H. Fowler, *Statistical Mechanics* (Cambridge University Press, Cambridge, 1966).